TITLE 1'AG11:

A new method for monitoring, the Earth's ionospheric total electron content using the GPS global network

A. J. Mannucci
B. D. Wilson
C. D. Edwards

for ION-GPS 93, September 22.-24, Salt Lake City, Utah.

1I1OGRA1'11Y

Anthony J. Mannucci is a member of the technical staff in the GPS Networks and Operations Group at the Jet Propulsion Laboratory in Pasadena, CA. He has spent the last four years developing and characterizing ionospheric calibration systems for deep space tracking and Earth-based satellite applications. He has over ten years of experience developing high accuracy measurement techniques in a variety of technical areas.

Brian Wilson, a member of the GPS Networks and operations Group at the Jet Propulsion Laboratory in Pasadena, CA, has been studying the ionosphere using Faraday rotation and GPS data for five years. He is the Cognizant Design Engineer of the current operational ionosphere calibration software for the Deep Space Network, which is based on single-site GPS data and is used to correct navigation radiometric data for media effects. He continues to pursue efforts to improve the calibration system and validate its accuracy by comparisons to independent ionosphere measurements such as Very Long Baseline Interferometry, integrated dual-frequency spacecraft Doppler, and the TOPEX dual-frequency altimeter. He is currently investigating the potential for using multi-site GPS datasets to produce hourly global ionospheric maps.

Charles (Chad) Edwards is currently the Manager of the Advanced Systems and Systems Development Programs in the Office of Telecommunication and Data Acquisition at Jet Propulsion 1 aboratory in Pasadena, CA. Prior to that he served as the Technical Supervisor of the Radio Metric Tracking Applications Group at JPI., where he was involved in developing and implementing high-accuracy deep-space tracking techniques, including precise ionospheric media calibrations based on GPS ground receiver observations. He has been at JPI, for nine years since receiving his Ph.D. in Physics from Caltech.

ABSTRACT

The global positioning system satellites and a world-wide network of dual-frequency GPS receivers can be used to measure ionospheric total electron content (TEC) on global scales. A new method for generating global TEC maps is described. This method uses a Kalman-type filter and random-walk process noise to generate TEC maps at time intervals of one hour or less. The maps utilize a locally-supported vertical TEC function (called "TRIN") based on tessellation of the sphere into 1280 spherical triangles. The 642 vertices of the triangles are assigned a TEC value estimated from the data and the TEC within each tile is computed by linearly interpolating between vertex TEC values. The previous approach used a single. - batch filter requiring an averaging time of 6-12 hours before a map could be obtained; the TEC data was fitted to a surface harmonic expansion which did not follow local TEC variations accurately. Both approaches usc a spherical thin-shell elevation mapping function to convert all station-to-satellite TEC measurements to equivalent vertical TEC at a unique shell intersect point. The new maps follow diurnal TEC variations over a single site to within a few TECU as measured by established single-site GPS calibration techniques. In a global-scale simulation using the Bent ionosphere model, the. TRIN fit reproduces the simulated data set to within 5 TECU over 70 percent of the globe. Errors exceeding 10 TECU are seen in the daytime-peak regions within the equatorial bulge. Methods for improving the accuracy of the maps are discussed.

1. INI'ROI)UCTION

The global positioning system (GPS) satellites and dual-frequency Earth-based receivers can be used to measure the total electron content (TEC) of the Earth's ionosphere. Global maps of vertical total electron content have been produced using the world-wide network of GPS receivers supported by the geodesy community (Wilson *et al.*, 1993). In this paper, a new method of generating such maps will be presented. Global ionospheric maps can be

used for calibrating single-frequency satellite altimetry missions and scientific investigations 01 the ionosphere. This may include. studies of the composition of the Earth's upper atmosphere, observing correlations between solar activity and ionospheric TEC, and correcting measurements of the geomagnetic field for ionospherically-induced electric currents.

The GPS global network (see figure 1) currently contains 454 stations which generate station-to-satellite range and phase observables at sub-minute intervals. This data is made readily available to researchers at JPL and elsewhere, Each station can track up to 8 satellites simultaneously, with a typical number being 6 satellites, hence there are roughly 240 lines of sight which probe the ionosphere simultaneously over the entire globe at every measurement interval.

The earlier technique for producing global maps from this data set required a waiting period of several hours before a fit could be performed (Wilson *et al.*, 1993). In this "single-bntch" approach, the ionosphere was assumed constant in a sun-fixed (local-time) reference frame and surface harmonic functions were used to fit the TEC measurements. In the approach reported here, a Kalman-typc filter is used allowing process noise to be included in the system model. In addition, fitting functions with local support at-c used allowing the maps to follow local TEC variations more accurately.

The method for converting GPS range observables into line of sight TEC (LOS-TEC) measurements will be discussed next, followed by a description of the global TEC model used for generating the maps. After a discussion of the parameter estimation strategy, results for selected time periods will be presented, along with a comparison to another GPS-based technique for ionospheric calibration.

2. DATA PRI1-PROCESSING

The first step in producing global maps is the conversion of the raw GPS range data to TEC measurements along the line of of sight. Once the TEC observable is formed, the original delay observables are no longer used. This pre-processing will be described followed by a discussion of the error sources which affect the accuracy of TEC extraction.

Formation of the TEC Observable

Two types of dc]ay observable are available from each station-to-satellite 10S measurement for the global network data: pseudorange delay (P) and earlier phase (L). Each observable is acquired at frequencies f_1 (1 .2276 GHz) and f_2 (1. S7542 GHz). The first step in data preprocessing is the application of the automated data-editing algorithm described by Blewitt (1990). An automated method is important for handling the large volume of data from a global data set. This algorithm can correct cycle slips in the phase data and identify outliers and earl-icr phase breaks. After processing by the automated algorithm, the edited raw data are divided into sets of phase-connected arcs.

For the pseudorange observables (P_1 and P_2), the difference in delay between the two frequencies is directly proportional to TEC expressed as the number of electrons per unit area:

$$\text{differential delay } (P_1 - P_2) \text{ in nanoseconds} = 2.85 \times 10^{16} \text{ el/m}^2 \quad (1)$$

Receiver and satellite clock errors in the pseudorange are removed in the differencing. The differential phase delay $(L_1 - L_2)$ is negative and, although inherently more precise than the pseudorange, is biased by an integer cycle ambiguity. This bias inconstant for each phase-connected arc of data, such as between a given satellite and receiver, but will differ from arc to arc,

The TEC observable is formed using both the pseudorange and carrier phase data in a process called "leveling": all the phase data for a single phase-connected arc is adjusted by a constant to match the absolute level of the pseudorange. The carrier phase is used because it is much more precise than the pseudorange.

The leveling process can be described as follows. Let N be the number of measurements in a phase-connected arc of data for a given receiver t and satellite s. For each datum i, the pseudorange delays are denoted by P_{1i}^{rs} and P_{2i}^{rs} for f_1 and f_2 frequencies respectively; the corresponding phase delays are L_{1i}^{rs} and L_{2i}^{rs}. The leveling bias B^{rs} is computed so as to minimize the root-sum-square difference between pseudorange and phase differential delay computed over the arc:

$$B^{rs} = \frac{1}{N} \sqrt{\sum_{i=1}^{N} \left\{ \left(P_{1i}^{rs} - P_{2i}^{rs} \right) - \left(L_{2i}^{rs} - L_{1i}^{rs} \right) \right\}^2} \quad (2)$$

The TEC observable for measurement i is the carrier phase difference $L_{2i}^{rs} - L_{1i}^{rs}$ added to the bias B^{rs}. After adjustment for the bias, the root-mean-square difference between the pseudorange and earlier phase delays, denoted D_{RMS}, is dominated by pseudorange noise.

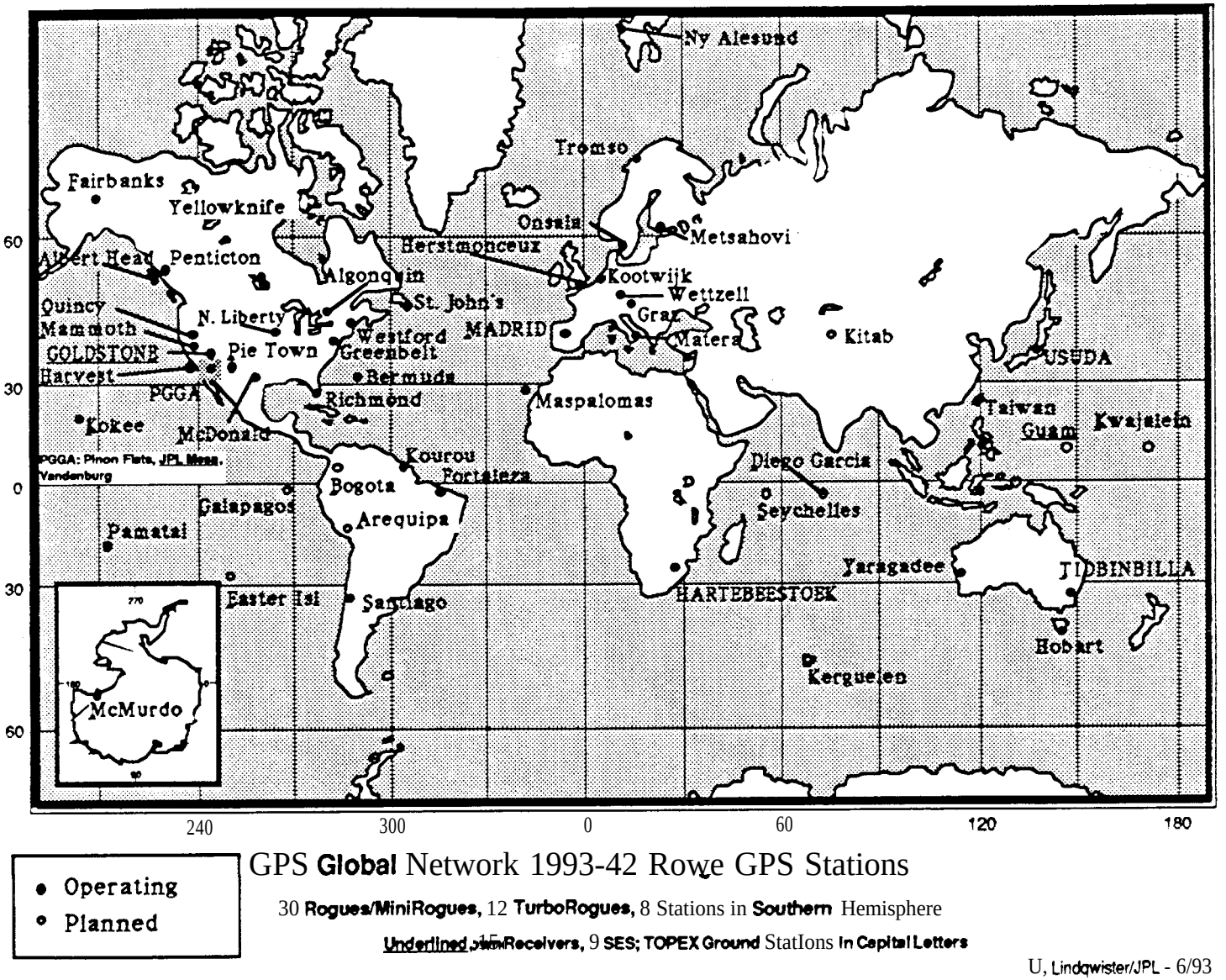

Figure 1. The global GPS network.

Error Analysis

There are several factors which limit the accuracy of the TEC observable derived above. These are:

- instrumental biases between frequencies) and f_2
- Multipath.
- Receiver noise.
- Antenna phase-center variations between f_1 and f_2.

Error estimates are shown in Table I in units of TEC units (1 TECU = 1×10^{16} electrons/m^2). For this study, parameters are for Rogue (SNR-8) receivers (Allen Osborne Associates, 1990). The global network data discussed in this paper is collected entirely from Rogue and Turbo-Rogue (SNR-8000) data.

The largest sources of error are typically the instrumental delay biases in both the satellites and receivers. These biases occur since different analog circuitry is used for processing the GPS signal at the two frequencies before digitization. Although large, these biases can be estimated in the global mapping process or calibrated for the receivers (Wilson and Mannucci,1993). The accuracy of [he TEC observable is not limited by the magnitude of these biases but rather the accuracy with which they can be estimated or measured.

The next largest source of error is from multipath effects. The TEC observable is sensitive to the *difference* in multipath between P_1 and P_2. The multipath error varies with elevation angle of the satellite and the physical configuration of the receiver site (presence of nearby reflecting surfaces, etc.). Since the pseudorange is roughly 1000 times more sensitive to multipath than the carrier phase, the RMS difference D_{RMS} between pseudorange and leveled carrier phase is a measure of the pseudorange multipath noise. The multipath estimate in Table 1 is the average value of D_{RMS} calculated from a several-day sample of global network data.

Errors from antenna phase center variations have been measured for the choke ring antennas used in the global network receivers by Young *et al.* (1993). These errors are not significant here. For the satellite antennas it is assumed that the errors are similar to those for the receiver antennas,

Weighting the Data

The data weight given to each individual TEC observation equals the. value of D_{RMS} for the phase-connected arc. If the multipath noise followed a Gaussian zero-mean distribution, the error in the TEC over an entire arc would be smaller than D_{RMS} by a factor of the square root of the number of points in the arc. Multipath noise is generally not zero-mean, particularly at the low elevations, so it is more conservative to give the TEC a data weight equal to the uncertainty of a single point in the arc, which on average equals D_{RMS}. Other error sources shown in Table I are not used in the data weight since they are much smaller than the pseudorange multipath noise.

Table 1: Errors affecting the TEC observable

Error Source		Error Estimate (TECU)
instrumental Biases--Satellite		-9 - +9(1)
Instrumental Biases--Receiver		-30 - +30(1)
Multipath Noise:	P-code	0,7 (2)
	Carrier Phase	<0.01
Receiver Noise:	P-code	0.13, T=5 min.
	Carrier Phase	<0.01
Antenna Phase Center Offset (1,1 vs. 1.2) Receiver		<o. I
Antenna Phase Center Offset (L1vs.L2) Satellite		<0.1

NOTES:
[1]The instrumental biases can be estimated from the data. Receiver biases can also be calibrated independently with an accuracy of 0.5 TECU (Wilson and Mannucci,1993).
[2]Varies with site and satellite geometry. Can be several TECU in extreme cases.

3. GLOBAL MAPPING TECHNIQUE

In this section, the technique used to produce global TEC maps will be described. It is assumed that a global TEC data set is available from the network using the pre-processing method described in the previous section. Creating a TEC map involves using the LOS TEC data to solve for a "global TEC function", or a specification of vertical TEC over all latitudes and longitudes for a given time. This function in effect serves to interpolate TEC between measurements which occur only at a discrete set of points.

Global TEC Model

We assume that the ionospheric electron density is concentrated on a thin shell of height $h = 350$ km above the mean Earth radius R_E. All slant TEC measurements are converted to an equivalent vertical value by using the thin shell elevation mapping function given by:

$$M(E) = \left\{1 - \left[\cos E / \left(1 + b/ R_E\right)\right]^2\right\}^{-1/2} \quad (3)$$

where E is the elevation of the *LOS* observation. The use of a mapping function is clearly an approximation, and can lead to errors of several TECU when applied to regions of large horizontal electron density gradients (Klobuchar *et al.*, 1993; Tsedilina and Weitsman, 1992). Mapping to vertical is necessary if the radial electron density structure is not modeled.

Every LOS measurement intersects the shell at a single latitude and longitude (θ, ϕ). The TEC measurements mapped to vertical are the input used to estimate a continuous global vertical TEC function. To define this function, the spherical surface is divided into 642 spherical triangles called tiles. The tiling is performed as follows. First, an icosahedron is projected onto the sphere, aligned such that two of the twelve vertices are at the north and south poles, and one of the non-polar vertices is aligned with the prime meridian. The twelve vertices define twenty equilateral spherical triangles on the sphere. Finer tiling is achieved by successive subdivisions of these spherical triangles. At each step, a given triangle is subdivided into four smaller triangles by bisecting each of the sides of the triangle and connecting the new vertices.

Let T_{rs} be a 1.0S TEC measurement between satellite s and receiver r with instrumental biases given by b_s and b_r. The "TRIN" (Triangular Interpolation) model assumes that T_{rs} **is given by the following expression:**

$$T_{rs} = \mathrm{M(E)} \sum_{\substack{i= \\ V_A, V_B, V_C}} W(\theta, \phi, i) V_i + b_r + b_s \quad (4)$$

where $M(E)$ is the mapping function (eqn. 3), Vi *is* the value of TEC at vertex i, and $W(\theta, \phi, i)$ are weighting functions for a shell intersect point having latitude and longitude (θ, ϕ). These functions relate the TEC values at the three vertices of a tile to the TEC at any point within a tile. The weighted sum in eqn. 4 is over the three vertices of the tile intersected by the observation.

The weighting $W(\theta, \phi, i)$ functions are defined by a linear interpolation algorithm which depends on the "great circle" distances between the shell intersect point and the vertex positions. The algorithm, depicted in Fig. 2, starts by drawing a great circle arc from vertex A through the point E=(θ, ϕ). This arc intersects the other side of the spherical triangle at point D. The values of TEC at vertices B and C are linearly interpolated to point D:

$$V_D = \frac{BD}{(BD + DC)} V_B + \frac{DC}{(BD + DC)} V_C \quad (5)$$

where BD is the arc length between points B and D and V_A is the TEC at vertex A etc. In a similar manner, the TEC is then interpolated linearly from points A and D to point E:

$$V_E = \frac{AE}{(AE + ED)} V_A + \frac{ED}{(AE + ED)} V_D \quad (6)$$

Equation (4) is used to calculate the observation partials for a linear least-squares parameter estimation strategy. A Kalman-type filter with the ability to estimate stochastic parameters is used to solve for b,, b, and all the V_i.

The vertex points which define the tiling are at fixed locations on the shell. Since the ionosphere is strongly

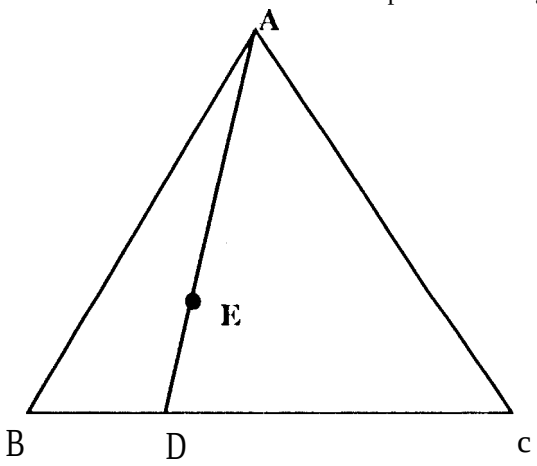

Figure 2: TRIN interpolation scheme

controlled by both the geomagnetic field and solar radiation, the coordinate system for the shell has been chosen to be the "solar-magnetic" system described in Knecht and Shuman (1985). The shell itself does not co-rotate with the Earth but is nearly fixed with respect to the Sun-Earth axis; a given longitude corresponds roughly to a given local time and the latitudes are geomagnetic. The z-axis of these coordinates is along the geomagnetic pole, chosen to intersect the Earth's surface at 78.5 N and 291.0 E. The y-axis is perpendicular to the both the pole and the Sun-Earth (local-noon) direction. The x-axis, which defines the zero of longitude, wobbles back and forth about the Earth-Sun direction by ±11.5 degrees as the Earth rotates.

Parameter Estimation Strategy

The parameters being estimated consist of the satellite and receiver instrumental delays b_r and b_s and the vertex TEC values V_i. Geometrical information about satellite orbits and station locations is known. In a typical computation, 642 vertex values are simultaneously estimated (this corresponds to 1280 tiles), along with about 40 receiver and 22 satellites biases. At least one receiver bias is held fixed to a known calibration value since otherwise the solution would be singular.

The instrumental delays are not expected to vary over the course of several days and are estimated as constants, Every vertex TEC parameter is governed by the following measurement update equation, which defines a random-walk process noise:

$$(V_i)_{j+1} = (V_i)_j + w \qquad (7)$$

where (V_i), is the value of vertex i estimated in data batch j, and w zero-mean white noise. The state transition matrix is the identity; no dynamical model for the vertex TEC is assumed and the global state estimate is determined solely from the data. The process noise is characterized by a standard deviation per root-second, σ_w, and affects the covariance of the state.

The process noise accounts for un-modeled TEC variations. The value for σ_w should equal the mean TEC change expected during one batch interval. It should be emphasized that temporal ionospheric changes, present even in solar-magnetic coordinates, are important. A comprehensive statistical analysis of ionosphere temporal statistics by region, local time and season is necessary for optimal determination of σ_w. Since such a database is not available, the value of σ_w has been estimated based on experience with the Bent model (Bent *et al.*, 1976) and a limited subset of data. The values used are presented with the results of the next section.

4. RESULTSAND D1SCLJSS1ON

In this section, a sample of results will be presented. The reasonableness of the mapping model will be demonstrated in two ways. First, the global map results will be used to compute vertical TEC directly over site as a function of time. This will be compared to the predictions of an established single-site ionospheric calibration technique (Lanyi and Roth, 1988). Second, a well-known empirical global model of the ionosphere will be used to generate a simulated data set which can be fit by the TRIN model. The results of the fit reveal weaknesses of the technique in the daytime ionosphere; possible improvements to TRIN will be discussed in the concluding section,

Sample Global Map: March 13, 1993, 12:00-13:00 UT

A representative global map and associated formal errors is shown in Fig.3. This map is derived from a data batch covering 1200-1300 UT. It is a smoothed solution using all the data above 20 degrees elevation from March 12 to March 14. Areas of the map appearing in black correspond to formal error standard deviations in excess of 10 TECU. These latitude bands contain too few receivers for adequate TEC estimation, Although the TEC map is created in a solar-magnetic reference frame, this map is plotted in sun-fixed shell coordinates and geographic latitude for simplicity. The stations translate horizontally underneath the sun-fixed shell as the Earth rotates, A land map is shown superimposed on the TEC map and the station locations are indicated as triangles on the formal error map.

The global map of Fig.3 shows prominent ionospheric features such as the equatorial anomaly and the difference between the day and nighttime ionospheres (in the map, local noon corresponds to zero degrees longitude), The peak of ionization occurs after local noon as expected.

The formal errors are determined by the TEC data weights, the observation geometry, the data equation, and the random-walk standard deviation σ_w. In this map, the same process noise was used for all of the vertices. A value of $3.56 \times 10^{-2} TECU/\sec^{1/2}$ was chosen allowing the model to follow TEC variations in the solar-magnetic frame of 2 TECU per hour. The batch interval was one hour.

Testing the TRIN Model Locally: Comparison with Single-Site Calibrations

One way of testing the TRIN model is to calculate the TEC predicted directly above a site using the global model and compare this to well-established single-site ionospheric calibration techniques. This allows testing of basic parameters of the model, such as vertex spacing (in the longitudinal direction) and batch interval. The global model should adequately track the diurnal TEC variations expected over a site. The single-site technique in this comparison is used operationally by NASA's Deep Space Network for ionospheric calibration of the DSN sites. The basis of this technique is described in Lanyi and Roth (1988), although the current operational system has added features which allow optimized calibrations along a given line-of-sight. Briefly, the ionosphere over a site is modeled as a second-degree polynomial in shell intersect angles (θ, ϕ), where sun-fixed shell coordinates are assumed. Observations are mapped to vertical using eqn. 3.

Three stations are shown in this comparison for March 13, 1993: a northern latitude station (Goldstone, CA) with neighboring stations within several hundred kilometers, a relatively isolated southern latitude station (Hartebeestok, South Africa) and an equatorial station (Kourou, French Guiana). The values of satellite and station biases used in the single-site fits were set equal to those determined in the global fits. The global fits were done using the same batch interval and process noise as the maps shown previously. As shown in Fig. 4, the agreement between TRIN and the single-site technique is usually within 2 TECU and differences never exceed 5 TECU. Similar comparisons using the older global surface harmonic technique were described in Wilson *et al.* (1993), where

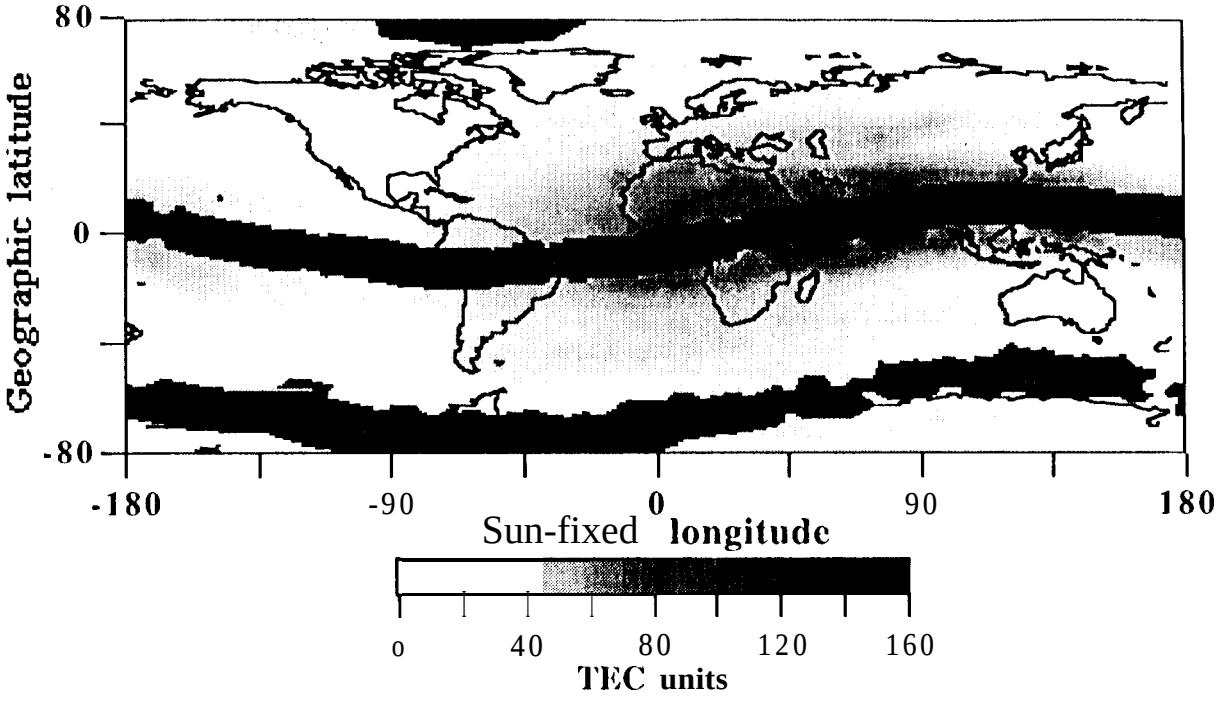

Figure 3a. The TRIN global TEC map for March 13, 1993 1200-1300 UT is shown. 'l'his map is a smoothed solution using three days of data, March 12-14, transformed to coordinates with sun-fixed longitude. A land map of the Earth in sun-fixed coordinates at 1230 UT is superimposed over the TEC map. Dark bands show areas where the formal error exceeds 10 TECU.

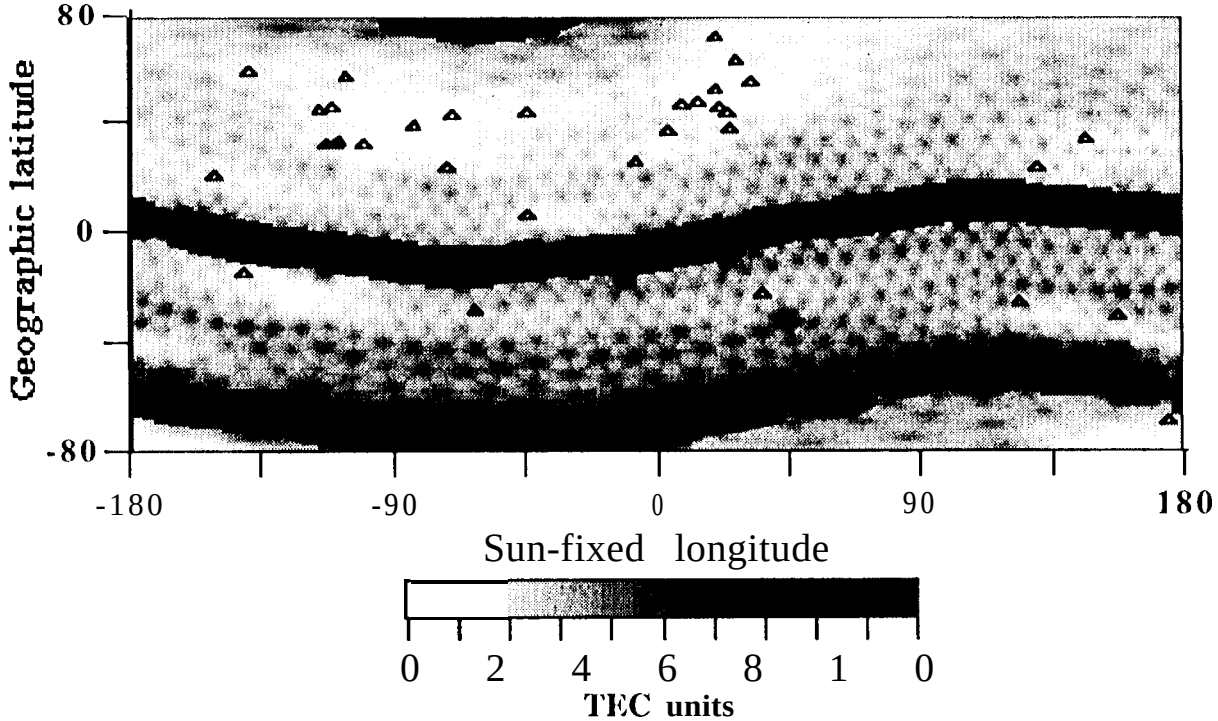

Figure 3b. The formal error map for March 13, 1993 1200-1300 UT is shown. Station locations in the sun-fixed coordinate system are shown as triangles. The black bands indicate regions where the formal error exceeds 10 TECU.

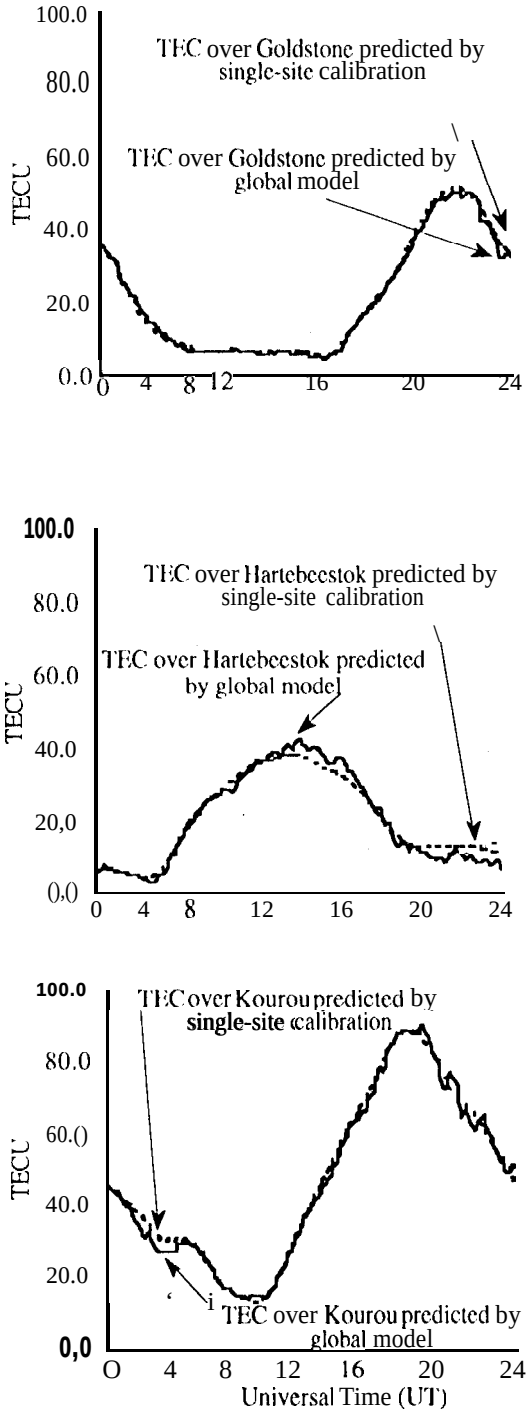

Figure 4. Comparisons between single-site and global TRIN fits for the TEC directly over a station as a function of time.

differences exceeding 10 TECU were common near the daytime peak.

Testing TRIN globally: Simulations using the Bent ionosphere Model

Another approach for testing the TRIN model is to generate a global data set using a good empirical model of the ionosphere. With a reasonable simulated data set, the fitted result can be compared directly to the model to determine which regions of the globe result in larger errors for TRIN.The simulated data set was created using the Bent ionospheric model (Bent *et al.*, 197(r) for three days centered on August 7, 1993. 1.0S TEC measurements were calculated for the satellite orbits anti station locations in existence on those days and an elevation angle cutoff of 20 degrees. First, the shell intersect coordinates of each measurement were computed assuming a shell height equal to the height of maximum ion density h_{max}, as specified by the Bent model. Vertical TEC was computed at that point. Then the vertical TEC was mapped to the 1.0S slant value assuming the thin-shell mapping function with shell height h_{max}. This approach is computationally simpler than a full integration of electron density profiles. However, the errors incurred using the thin shell approximation are not ascertained.

The absolute magnitude of the difference between the simulated global TEC and the TRIN global fit is shown as a map in Fig. 5 for a data batch of 1200-1215 UT. As in the previous global map, this map is a smoothed solution, using simulated data from August 6-8. The batch interval was 15 minutes and the process noise sigma was 5.1×10^{-2} *TECU* / $\sec^{1/2}$ (1.25 TECU per 15 minutes) for vertices above 35 degrees latitude and 8.3×10^{-2} *TECU* / $\sec^{1/2}$ (2.5 TECU per 15 minutes) for vertices within 35 degrees of the magnetic equator. These values were chosen based on the change in TEC predicted by the Bent model over 15 minutes. For over 70 percent of the globe, the agreement is quite good (within 5 TECU), but in certain regions particularly around the equator and daytime peak the errors exceed 10 TECU. The equatorial and high-latitude white strips represent regions where the formal errors exceed 10 TECU due to lack of coverage.

There arc two causes for the areas of poor agreement in Fig. 5. First, the vertex points are too far apart in the meridional direction to follow the large TEC variations near the equatorial anomaly. Second, when the stations are widely separated, time variability causes errors because the TEC is not updated in the absence of data. Methods for overcoming these limitations are currently under study.

5. CONCLUSIONS

A new method of using the GPS global network for global ionospheric monitoring has been presented. Global TEC maps are produced with time resolutions of less than one hour by using a linear least-squares parameter estimation procedure with the addition of process noise,.

The maps are generated within the context of a single-layer (bin shell model, and are parametrized by a set of vertex TEC values distributed uniformly over the shell. A linear interpolation scheme based cm spherical triangles, or tiles, is used to define the global TEC function.

Comparisons between the global TRIN (TRiangular interpolation) method and established single-site calibration techniques reveal that the model is adequate to follow the expected diurnal TEC changes over a site. In a comparison with a simulated global data set, the maps were found to give good agreement over most of the globe. The worst performance was found in the daytime regions near the equatorial bulge, where horizontal TEC gradients arc large and the ionosphere is highly time variable. More validation work is needed, particularly with a data set which is independent of GPS ionospheric measurements.

The current monitoring technique can be improved in several ways. 1 'irst, the ionosphere model can be extended to include information about the radial distribution of electron density so that the TEC observable can be correctly modeled by integrating ionospheric densities along the line of sight. Second, the vertex spacing can be changed to reflect the higher meridional gradients which exist near the equatorial bulge. Using equally-spaced vertices is not optimal due to the large persistent structural features which occur in the ionosphere, Third, a smoother global TEC function can be adopted. The function used in this work is continuous but does not have continuous derivatives. Enforcing higher-order continuity will increase the number of vertex parameters affected by a given observation, and improve the ability of the model to bridge the data gaps where station coverage is limited.

ACKNOWLEDGMENTS

This analysis was made possible by the high quality of the global GPS data set, the result of a collaborative effort involving many people at JPL anti al other centers around

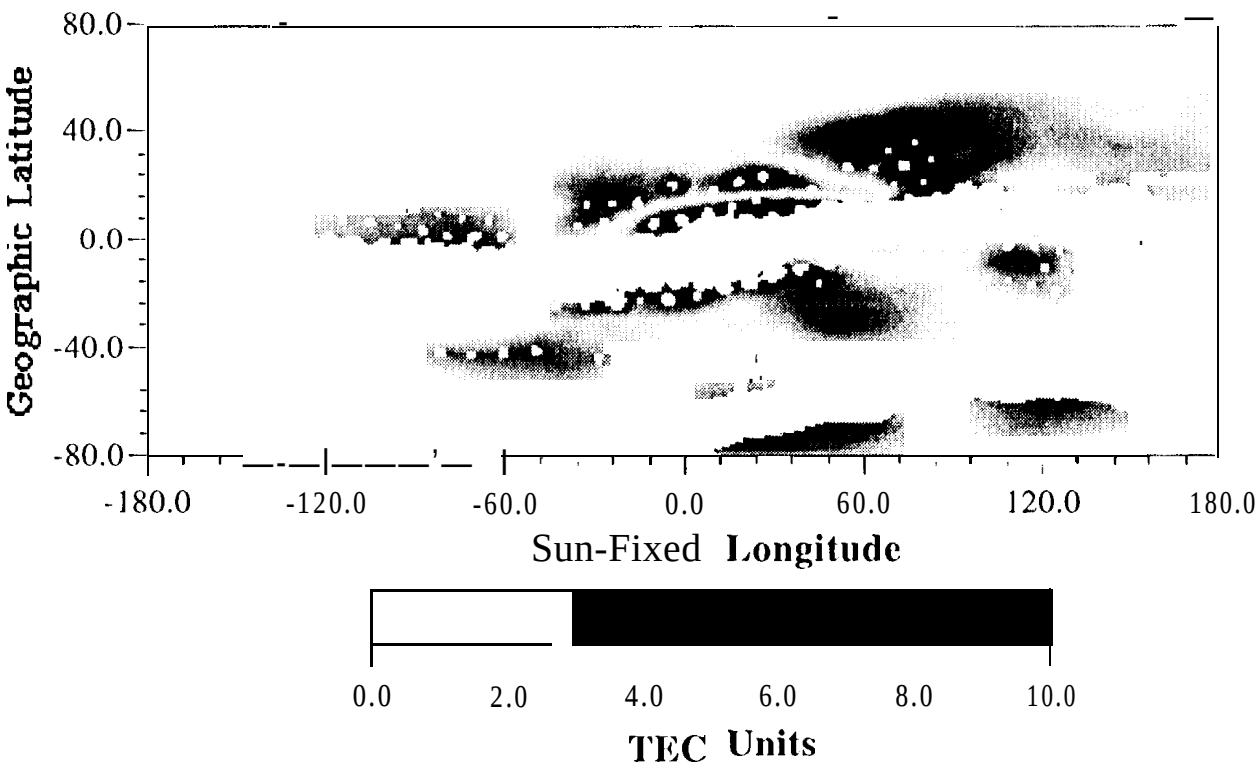

Figure 5. The difference (absolute value) between the TRIN fit to the Bent ionosphere model and the Bent ionosphere for August 7, 1993 is shown. The fit is for 1200-1215 U'I', shown in sun-fixed shell coordinates. This is a smoothed solution using data from August 6-8. The TRIN global map is subtracted from the simulated Bent TEC global model of 1207 UT, using the reai network and satellite positions for August 6-8, 1993. White banded areas in the equatorial and high-latitude regions areas where the formal error exceeds 10 TECU.

the world. We also with to express our appreciation to Ulf Lindqwister, Tom Runge and Herb Royden for helpful discussions and suggestions. A debt of gratitude is owed to Ron Muellerschoen for his advice on use of the GIPSY filtering software and his modifications to it for our purposes. The research described in this paper was performed by the Jet Propulsion Laboratory, California institute of I'ethnology, under contract with the National Aeronautics and Space Administration,

REFERENCES

Allen Osborne Associates (1990) Specification sheet for the SNR-800 Rogue receiver, **AOA-9-15-90**, Westlake Village., CA.

Bent, R. B., Llewellyn, S. K., Nesterczuk, G., Schmid, P. E., (1976) The development of a highly successful world-wide empirical ionospheric model and its use in certain aspects of space communications and world-wide total electron content investigations, *Effect of the Ionosphere on Space Systems and Communications,* J. Goodman. cd., Springfield, VA, 1976.

Blewitt, G. (1990) An automated editing algorithm for GPS data, *Geophysical Research Letters, 17,* 199-202.

Klobuchar, J. A., Basu, S., Doherty, P. (1993) Potential limitations in making absolute ionospheric measurements using dual frequency radio waves from GPS satellites, *Proceedings of the Seventh International Ionospheric Effects Symposium*, J. Goodman, cd., Alexandria, VA, May 1993,

Knecht, D. J., Shuman, B. M. (1985) The geomagnetic field, *Handbook Of Geophysics and the Space Environment,* A. S. Jursa, cd., Air Force Geophysics Laboratory.

Lanyi, G. E., Roth, T. (1988) A comparison of mapped and measured total ionospheric electron content using global positioning system and beacon satellite observations, *Radio Science*, 23, 483-492,

Tsedilina, E. E., Weitsman, O. B. (1992) influence of the inhomogeneous ionosphere on the GPS determination of satellite and user coordinates, *43rd Congress of the International Astronautical Federation*, Washington I). C., August 1992.

Wilson, B. D., Mannucci, A. J., Edwards, C. D. (1993) Sub-daily northern hemisphere ionospheric maps using the IGS GPS network, *Proceedings of the Seventh International Ionospheric Effects Symposium*, J. Goodman, cd., Alexandria, VA, May 1993.

Wilson, B. I)., Mannucci, A. J. (1993) Instrumental biases in ionospheric measurements derived from GPS data, to appear in *Proceedings of Institute of Navigation GPS-93*, Salt Lake City, Utah, September, 1993.

Young, 1,. 11., Munson, T. N., Dunn, C. E., Davis, E. S. (1993) GPS precision orbit determination: measured receiver performance, submitted to Geophysical Research Letters.